Application of Unsupervised Clustering Methods to Medical Imaging

A. Meyer-Baese[1], F.J. Theis[2], P. Gruber[2], A. Wismueller[1] and H. Ritter[3]
[1]Florida State University, Tallahassee, USA
[2] University of Regensburg, Regensburg, Germany
[3] University of Bielefeld, Bielefeld, Germany
amb@eng.fsu.edu

Abstract - *Unsupervised clustering techniques represent a powerful technique for self–organized segmentation of biomedical image time–series data describing groups of pixels exhibiting similar properties of local signal dynamics. The theoretical background is presented in the beginning, followed by several medical applications demonstrating the flexibility and conceptual power of these techniques. These applications range from functional MRI data analysis to dynamic contrast–enhanced perfusion MRI and breast MRI. The present paper gives a review of potential applications of unsupervised clustering techniques in the important and current field of functional and dynamic MRI.*

Key words - Unsupervised clustering, fMRI, MRI, dynamic perfusion MRI

1 Introduction

In the last decades, several advanced noninvasive medical imaging techniques such as magnetic resonance imaging (MRI) and functional MRI (fMRI) have been introduced into clinical practice. These new techniques are not only limited to the mere imaging of morphological structures but also emphasize the biological function. As a consequence, the analysis and visualization of medical image time–series data poses a new challenge to both basic research and medical application. The model–based, supervised data analysis methods rely on knowledge of experimental conditions and model assumptions whereas model–free techniques do not. However, model–based analysis methods impose some limitations on data analysis under complicated experimental conditions. Therefore, analysis methods that do not rely on any assumed model are considered more powerful and relevant.
In this important context, we apply unsupervised clustering methods to biomedical image time–series analysis and present applications of these techniques to (i) fMRI data analysis for human brain mapping, (ii) dynamic contrast–enhanced perfusion MRI for the diagnosis of cerebrovascular disease and (iii) breast MRI for the segmentation of suspicious lesions of breast cancer patients.
In the following we will give a review on unsupervised clustering algorithms to be applied to fMRI and MRI exploratory data analysis, and introduce some basic notations common to all three applications.

Let n denote the number of subsequent scans in a fMRI or dynamic MRI study, and let M be the number of pixels in each scan. The dynamics of each pixel $\mu \in \{1, \ldots, M\}$, i.e. the sequence of signal values $\{x^\mu(1), \ldots, x^\mu(n)\}$ can be interpreted as a vector $\mathbf{x}^\mu \in \mathbf{R}^n$ in the n–dimensional feature space of possible signal time–series at each pixel (Pixel Time Course, PTC).
Cluster analysis groups image pixels together based on the similarity of their intensity profile in time. In the clustering process, the space of all PTCs is subsequently partitioned into clusters based on the proximity of the input data. For this, we employ several vector quantization (VQ) approaches. method for unsupervised image time–series analysis. VQ clustering identifies several groups of pixels with similar PTC, while these groups or clusters are represented by prototypical time–series called codebook vectors (CV) located at the center of the corresponding clusters. The CVs represent prototypical PTCs sharing similar temporal characteristics. Thus, each PTC can be assigned to a specific CV according to a minimal distance criterion.

2 Unsupervised clustering techniques

As unsupervised clustering techniques, we will consider adaptive neural algorithms such as topology–preserving and neighborhood–preserving mappings.
By $X \subseteq R^D$ we describe an input manifold (D is the dimension of the input space) and by G we describe a graph or equivalently a network. This graph G consists of vertices $i \in \{1, \cdots, c\}$, which are equivalent to neurons. A reference vector $\mathbf{w}_i \in X$ belongs to the pointer set or codebook $C = \{\mathbf{w}_1, \cdots, \mathbf{w}_c\}$ attached to the vertex i.
A mapping ϕ_T for codebook C from input manifold X onto the vertices of graph G is defined as

$$\phi_T : X \to G, \quad \mathbf{x}_k \in X \to i^*(\mathbf{x}_k) \in G \tag{1}$$

with $\mathbf{x}_k$ being an input vector, $k \in \{1, \ldots, n\}$ and vertex $i^*(\mathbf{x}_k)$ a winner unit determined by the minimized Euclidian inter–vector distance selecting the pointer $\mathbf{w}_{i^*(\mathbf{x}_k)}$ closest to $\mathbf{x}_k$

$$i^*(x_k) = arg \min_{i \in G} d(x_k, w_i) \tag{2}$$

Similarly, an inverse mapping ϕ_T^{-1} from G onto X is defined as

$$\phi_T^{-1} : G \to X, \quad i \in G \to \mathbf{w}_i \in X \tag{3}$$

For a more detailed discussion of topology preservation in the context of vector quantization approaches, see [7]. The mapping ϕ_T from X to G is defined as neighborhood (adjacency) preserving if any pair of adjacent pointers $\mathbf{w}_i, \mathbf{w}_j$ on X is assigned to vertices i, j also adjacent on G. Vice versa, mapping ϕ_T^{-1} is said to be neighborhood preserving if any two vertices i, j adjacent on G are assigned to locations $\mathbf{w}_i, \mathbf{w}_j$ that are adjacent on X. In this context, a topology preserving mapping is defined as a mapping ϕ_T from X to G such that ϕ_T, together with inverse mapping ϕ_T^{-1} from G to X are neighborhood (adjacency) preserving.
Cluster centers or codebook vectors (CV) $\mathbf{w}_i$ are then determined by an iterative adaptive update based on the following equation:

$$\mathbf{w}_i(t+1) = \mathbf{w}_i(t) + \epsilon(t) a_{i,i^*}(\mathbf{x}(t), C(t), \kappa)(\mathbf{x}(t) - \mathbf{w}_i(t)) \tag{4}$$

where $\epsilon(t)$ represents the learning parameter, a_{i,i^*} a codebook ($C(t)$) dependent cooperativity function, κ a cooperativity parameter, and $\mathbf{x}$ a randomly chosen feature vector. For image time–series, the feature vector represents the PTC.
Kohonen's self–organizing map generates nodes on a two–dimensional lattice in which the distribution of these nodes corresponds to the proximity of their associated node patterns in the signal intensity space. This topology–preserving technique enables the forming of superclusters by fusing nodes, and thus provides a way to visualize high–dimensional data sets.
The learning rule for the Kohonen's self–organizing map uses the simple cooperativity function $a_{i,i^*} = \exp\left(-\frac{d_{ij}}{\sigma^2}\right)$ and is given by

$$\mathbf{w}_i(t+1) = \mathbf{w}_i(t) + \epsilon(t) \exp\left(-\frac{d_{ij}}{\sigma^2}\right)(\mathbf{x}(t) - \mathbf{w}_i(t)) \tag{5}$$

where d_{ij} is a distance between neurons i and j determined by a neighborhood relation and σ^2 is a range parameter. Note that $\exp\left(-\frac{d_{ij}}{\sigma^2}\right)$ takes the maximum value of one for $i = i^*$, namely for the best–match neuron, and decreases when the distance becomes large.
Another tool for the analysis of biomedical time–series is given by the minimal free energy vector quantizer also known as fuzzy clustering technique based on deterministic annealing [4]. The learning rule for the minimal free energy vector quantizer is given by

$$\mathbf{w}_i(t+1) = \mathbf{w}_i(t) + \epsilon(t) \frac{\exp(-||\mathbf{x}(t) - \mathbf{w}_i(t)||^2/2\rho^2)}{\sum_i \exp(-||\mathbf{x}(t) - \mathbf{w}_i(t)||^2/2\rho^2)}(\mathbf{x}(t) - \mathbf{w}_i(t)) \tag{6}$$

where ρ is the 'fuzzy range' of the model, and defines a length scale in data space and is annealed to repeatedly smaller values in the VQ approach. In parlance of statistical mechanics, ρ represents the temperature T of a multiparticle system by $T = 2\rho^2$.
The employed cooperativity function

$$a_{i,i^*} = \frac{\exp(-||\mathbf{x}(t) - \mathbf{w}_i(t)||^2/2\rho^2)}{\sum_i \exp(-||\mathbf{x}(t) - \mathbf{w}_i(t)||^2/2\rho^2)} \tag{7}$$

is the so–called softmax activation function, and accordingly the outputs lie in the interval [0,1] and they sum up to one. In deterministic annealing some form of randomness is incorporated into the energy function itself, which is then deterministically optimized at a sequence of decreasing temperatures [4]. The algorithm starts with one cluster representing the center of the whole data set. Gradually, the large clusters split up into smaller ones representing smaller regions in the feature space.
The 'neural-gas' algorithm [2] is an efficient approach which, applied to the task of vector quantization, (1) converges quickly to low distortion errors, (2) reaches a distortion error [2] lower than that from Kohonen's feature map, and (3) at the same time obeys a gradient descent on an energy surface.

[2]This error measures the fidelity of data encoding, and is given by the squared Euclidean distance between the data vectors and the corresponding approximating reference vectors.

Instead of using the distance $||\mathbf{x} - \mathbf{w_i}||$ or of using the arrangement of the $||\mathbf{w_i}||$ within an external lattice, it utilizes a neighborhood–ranking of the reference vectors $\mathbf{w_i}$ for the given data vector $\mathbf{x}$.
The learning rule for the neural gas network performs VQ using the cooperativity function $a_{i,i^*} = \exp(-k_i(\mathbf{x}, \mathbf{w_i}/\lambda))$ and is given below

$$\mathbf{w}_i(t+1) = \mathbf{w}_i(t) + \epsilon(t) \exp(-k_i(\mathbf{x}, \mathbf{w_i})/\lambda)(\mathbf{x}(t) - \mathbf{w}_i(t)) \tag{8}$$

where $k_i = 0, \ldots, N-1$ represents the rank index describing the 'neighborhood–ranking' of the reference vectors $\mathbf{w_i}$ to the data vector $\mathbf{x}$ in a decreasing order, N is the number of units in the network, and λ determines the number of neural units significantly affected by every iteration. The step size $\epsilon \in [0, 1]$ describes the overall extent of the modification.
It can be shown [2] that the average change of the reference vectors corresponds to an over-damped motion of particles in a potential that is given by the negative data point density. Superimposed on the gradient of this potential is a 'force', which points toward the regions of the space where the particle density is low. This force is the result of a repulsive coupling between the particles (reference vectors). In its form it resembles an entropic force and tends to homogeneously distribute the particles (reference vectors) over the input space, like the case of a diffusing gas. This suggests the name for the neural-gas algorithm. It is interesting to also mention that the reference vectors $\mathbf{w_i}$ change their locations slowly but permanently and that vectors $\mathbf{w_i}$ which are neighboring at an early stage of the adaptation procedure might not be neighboring anymore at a more advanced stage.

3 Functional MRI

Functional magnetic resonance imaging with high temporal and spatial resolution represents a powerful technique for visualizing rapid and fine activation patterns of the human brain. As is known from both theoretical estimations and experimental results [3], an activated signal variation appears very low on a clinical scanner. This motivates the application of analysis methods to determine the response waveforms and associated activated regions. Generally, these techniques can be divided into two groups: model-based and model-free techniques. The first try to exploit the data structure as well as possible by requiring prior knowledge about activation patterns, whereas the latter are exploratory in nature and do not need additional assumptions. Under complicated experimental conditions, modeling is often difficult to achieve. Therefore, analysis methods that do not rely on any assumed model of functional response are considered more powerful and relevant.
FMRI data were recorded from six subjects (3 female, 3 male, age 20-37) performing a visual task. In five subjects, five slices with 100 images (TR/TE=3000/60msec) were acquired with five periods of rest and five photic simulation periods with rest. Simulation and rest periods comprised 10 repetitions each, i.e. 30s. Resolution was $3 \times 3 \times 4$ mm. The slices were oriented parallel to the calcarine fissure. Photic stimulation was performed using an 8 Hz alternating checkerboard stimulus with a central fixation point and a dark background with a central fixation point during the control periods. The first scan was discarded for remaining saturation effects. Motion artifacts were compensated by automatic image alignment.
Clustering the PTC identifies groups of pixels with similar signal dynamics. The clustering results for the neural gas algorithm are shown exemplarily in Figure 1. Figure 1(a) illus-

trates the so–called assignment maps where all the pixels belonging to a specific cluster are highlighted. The assignment between a pixel and a specific cluster is given by the minimum distance between the pixel and a CV from the established codebook. On the other hand, each CV shown in Figures 1(b) can be viewed as the cluster–specific weighted average of all pixel time courses.
The first two codebook vectors in Figure 1(b) are similar to the rectangular pulse–like stimulus function. Their corresponding cluster assignment maps in Figure 1 (a) can be attributed to activation of the visual cortex [5].

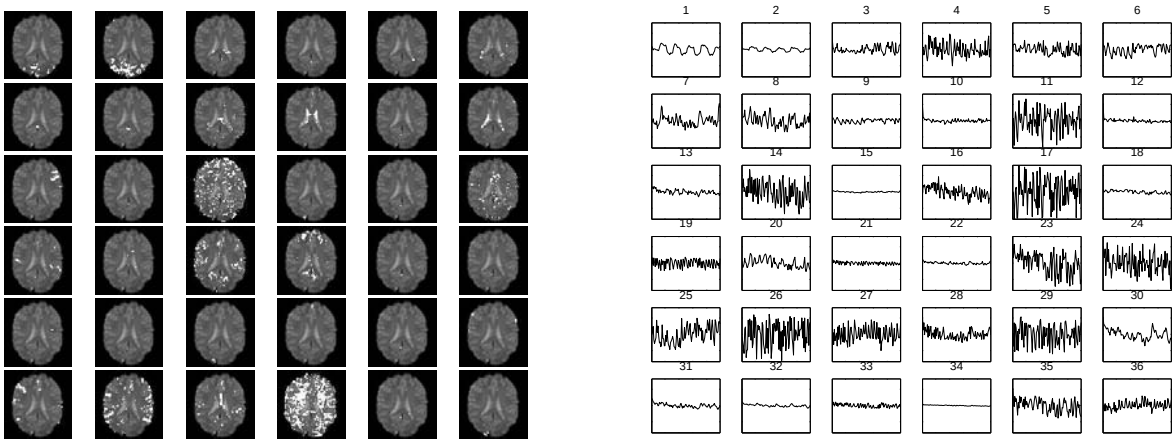

(a) (b)

Figure 1: (a) Cluster assignment maps for cluster analysis based on the neural gas network of a visual stimulation fMRI experiment obtained for 36 CVs. (b) Associated codebook vectors for the neural gas network clustering as shown in (a). Assignment of the codebook vectors corresponds to the order of the assignment maps shown in (a).

4 Dynamic contrast–enhanced MRI mammography

Breast cancer is the most common cancer among women. When applied to segmentation of breast MR images, traditional pattern recognition techniques such as the MLP have shown unsatisfactory detection results and limited application capabilities [1]. Furthermore, the underlying supervised nonbiological learning strategy leads to the incapacity of capturing the feature structure of the breast lesion in the neural architecture.
To overcome the above mentioned problem, we employ a minimal free energy vector quantization neural network that focusses strictly on the observed complete MRI signal time–series, and enables a self–organized data–driven segmentation of dynamic contrast–enhanced breast MRI time–series with respect to fine–grained differences of signal amplitude and dynamics such as focal enhancement in patients with indeterminate breast lesions. This method is developed, tested and evaluated for functional and structural segmentation, visualization, and classification of dynamic contrast–enhanced breast MRI data. Thus, we contribute towards the construction and evaluation of a flexible and reusable software system for CAD in breast MRI [6].
MRI was performed with a 1.5 T system (Magnetom Vision, Siemens, Erlangen, Germany)

equipped with a dedicated surface coil to enable simultaneous imaging of both breasts. The patients were placed in a prone position.
The dynamic study consisted of 6 measurements with an interval of 83 s. The first frame was acquired before injection of paramagnetic contrast agent (gadopentatate dimeglumine, 0.1 mmol/kg body weight, Magnevist^{TM}, Schering, Berlin, Germany) immediately followed by the 5 other measurements. The initial localization of suspicious breast lesions was performed by computing difference images, i.e. subtracting the image data of the first from the fourth acquisition. As a preprocessing step to clustering, each raw gray level time–series $S(\tau), \tau \in \{1, \cdots, 6\}$ was transformed into a PTC of relative signal reduction $x(\tau)$ for each voxel, the pre–contrast scan at $\tau = 1$ serving as reference.
Clustering results for a 6 scan dynamic contrast–enhanced breast MRI study in a patient with breast cancer in the upper medial quadrant of the left breast are presented in Figure 2 for the neural gas network employing 9 clusters. They show cluster assignment maps and corresponding codebook vectors of breast MRI data covering a supramammilar transversal slice of the left breast containing a suspicious lesion that has been proven to be malignant by subsequent histological examination.
The procedure is able to segment the lesion from the surrounding breast tissue as can be seen clusters #6 from Figure 2(a). The rapid and strong contrast agent uptake followed by subsequent plateau and wash–out phases in the round central region of the lesion as indicated by the corresponding CV of cluster #6 in Figure 2(b).
Furthermore, clustering results enable a subclassification within this lesion with regard to regions characterized by different MRI signal time–courses: The central cluster #6 is surrounded by the peripheral circular clusters #7, 8, and 9 which primarily can be separated from both the central region and the surrounding tissue by its amplitude of its contrast agent uptake ranging between CV #6 and all the other CVs. Analysis of the resulting data can be further aided by the use of hyperbolic SOMs for the VQ and coloring steps [8].

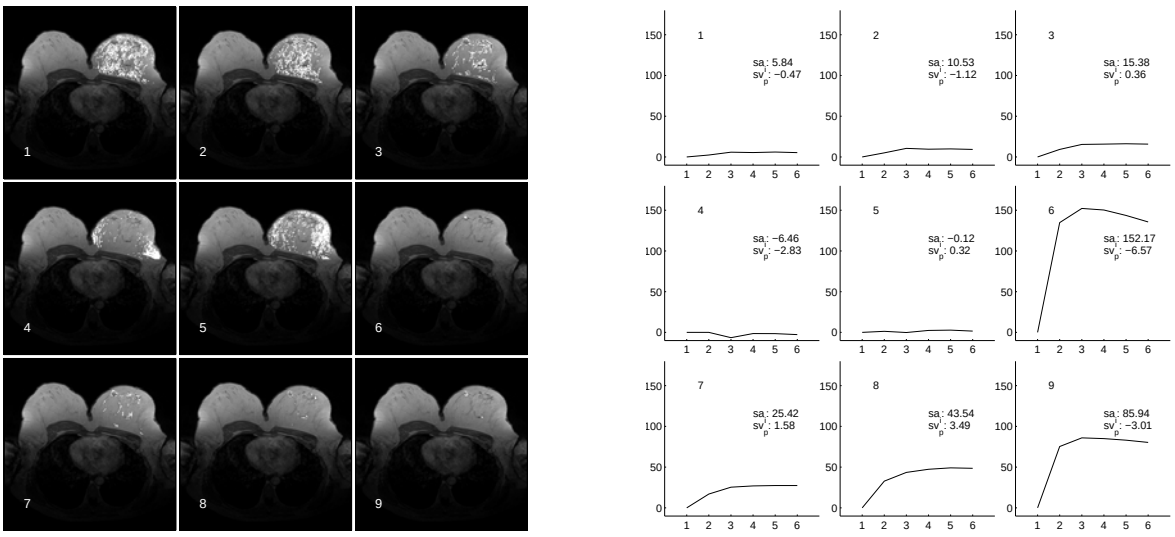

Figure 2: (a) Cluster assignment maps for cluster analysis based on the minimal free energy vector quantization of the dynamic breast MRI study (data set #16). (b) Codebook vectors for minimal free energy vector quantization of the dynamic breast MRI study according to (a). sa_i represents the initial and sv_p the postinitial time–signal intensity.

5 Dynamic contrast–enhanced cerebral perfusion MRI

Stroke and cerebrovascular diseases are the third leading cause of mortality in industrial countries after cardiovascular disease and malignancies. Therefore, the analysis of cerebral circulation, has become an issue of enormous clinical importance. The main objective of dynamic contrast–enhanced MRI is to separate abnormal from normal contrast enhancement reflecting disturbed hemodynamics.

Dynamic susceptibility contrast-enhanced perfusion weighted MRI was performed on a 1.5 T system (Magnetom Vision, Siemens, Erlangen, Germany) using a standard circularly polarized head coil for radio frequency transmission and detection.

Clustering results for a 38 scan dynamic contrast-enhanced MRI perfusion study in a patient with a subacute stroke affecting the right basal ganglia are presented in Figure 3. After discarding the first two scans, a relative signal reduction time–series $x(\tau), \tau \in \{1, \ldots, n\}, n = 36$ can be computed for each voxel. Clustering these PTCs identifies groups of pixels with similar signal dynamics. Figure 3(a) shows the cluster assignment maps overlaid onto an EPI scan of the perfusion sequence. In these maps, all the pixels are highlighted that belong to a specific cluster. The decision on assigning a pixel μ characterized by the PTC $\mathbf{x}^\mu = (x^\mu(\tau)), \tau \in \{1, \ldots, n\}$ to a specific cluster j is based on a minimal distance criterion in the n-dimensional time–series feature space, i.e. μ is assigned to cluster j, if the distance $\|\mathbf{x}^\mu - \mathbf{w}_j\|$ is minimal, where $\mathbf{w}_j$ denotes the CV belonging to cluster j. Each CV can be interpreted as the weighted centroid of all the PTCs belonging to this cluster.

Figure 3(b) shows the prototypical cluster-specific concentration-time curves (CTCs) belonging to the pixel clusters of Figure 3(a).

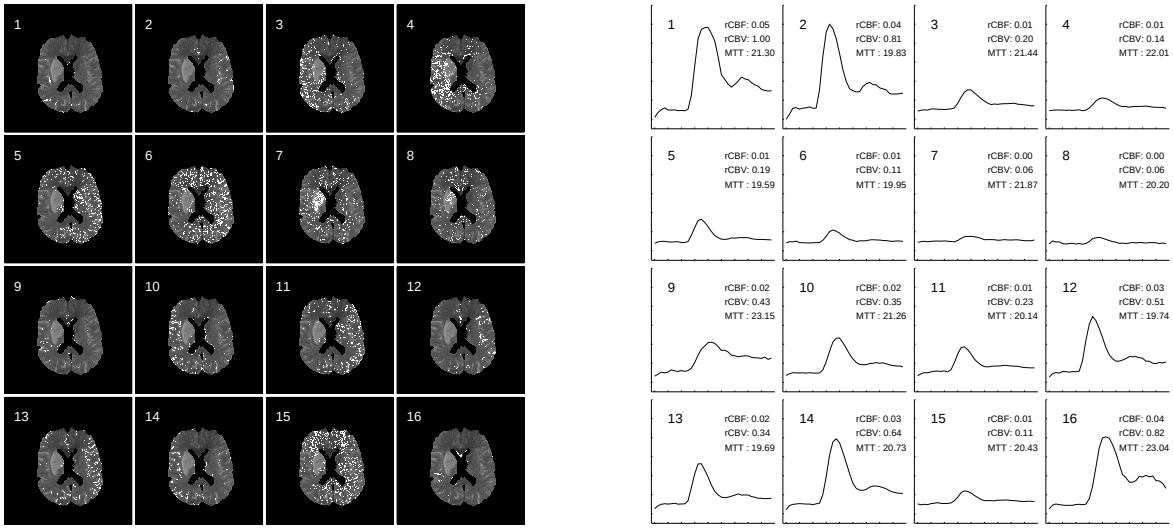

Figure 3: (a) Cluster assignment maps for neural gas network of a dynamic perfusion MRI study in a patient with stroke in the right basal ganglia. (b) Cluster-specific concentration-time curves for neural gas network of a dynamic perfusion MRI study in a patient with stroke in the right basal ganglia. Cluster numbers correspond to (a). MTT values are indicated as multiples of the scan interval (1.5s), rCBV values are normalized with respect to the maximal value (cluster #9).

6 Conclusion

In the present paper, we have shown that unsupervised clustering algorithms represent a successful strategy for the analysis of biomedical imaging time–series: they identify activated brain regions in fMRI studies and provide an accurate segmentation in dynamic MRI regarding either identification of regions of perfusion deficit in patients with stroke or identification and subclassification of pathological breast tissue lesions.
The goal of this review paper was to demonstrate the robustness and reliability of extracting task–related activation maps and time–courses from fMRI and dynamic MRI data sets based on unsupervised clustering techniques. The applicability of the unsupervised clustering algorithms is illustrated on experimental data.
In future works, clinical studies will have to reveal the broad applicability of the novel concepts of model-free data analysis to these common imaging problems.

References

[1] E. Lucht and M. Knopp and G. Brix (2001), Classification of signal-time curves from dynamic (MR) mammography by neural networks, *Magnetic Resonance Imaging*, **vol. 19**, p. 51-57.

[2] T. Martinetz and S. Berkovich and K. Schulten (1993), Neural Gas Network for Vector Quantization and its Application to Time–Series Prediction, *IEEE Transactions on Neural Networks*, **vol. 4**, p. 558-569.

[3] S. Ogawa and T. Lee and B. Barrere (1993), The sensitivity of magnetic resonance image signals of a rat brain to changes in the cerebral venous blood oxygenation activation, *Magn. Reson. Med.*, **vol. 29**, p. 205-210.

[4] K. Rose and E. Gurewitz and G. Fox (1992), Vector Quantization by Deterministic Annealing, *IEEE Transaction on Information Theory*, **vol. 38**, p. 1249-1257.

[5] A. Meyer-Baese and A. Wismueller and O. Lange (2004) Comparison of Two Exploratory Data Analysis Methods for fMRI: Unsupervised Clustering versus Independent Component Analysis, *IEEE Transactions on Information Technology in Biomedicine*, **vol. 8**, p. 387-398.

[6] A. Meyer-Baese and A. Wismueller and O. Lange and G. Leinsinger (2004), Computer-Aided Diagnosis in Breast MRI Based on Unsupervised Clustering Techniques, *Proceedings of SPIE*, **vol. 5421**, p. 29-37.

[7] H. Bauer and M. Herrmann and T. Villmann (1999) Neural maps and topographic vector quantization, *Neural Networks*, **vol. 12**, p. 659-676.

[8] A. Saalbach and J. Ontrup and H. Ritter and A. Wismueller and T. Nattkemper (2005) Image Fusion based on Topographic Mappings using the Hyperbolic Space, *Information Visualization*, in press.